Figure S1

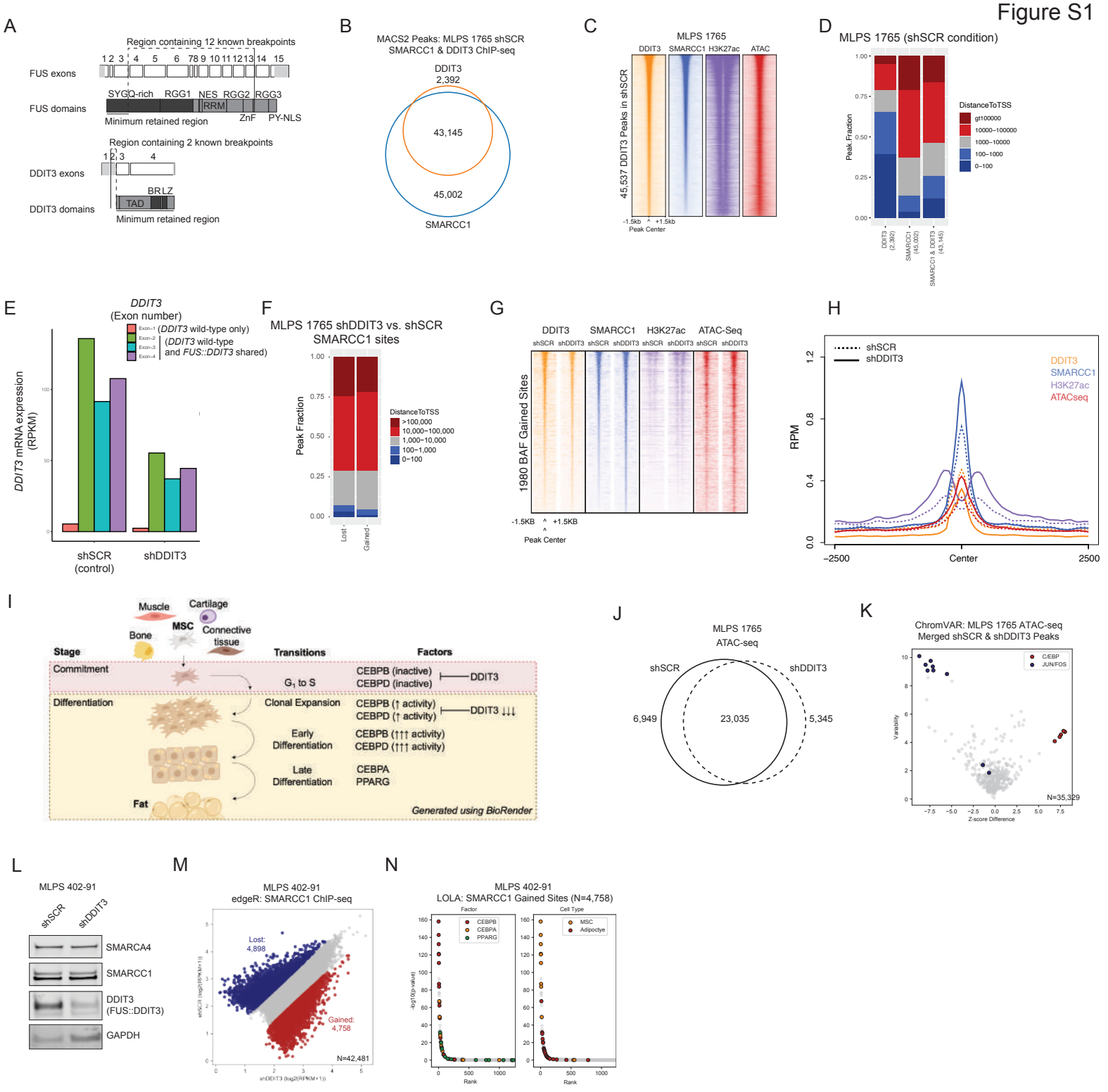

Figure S1. FUS::DDIT3 colocalizes with BAF complexes at promoter-proximal sites, while inhibiting BAF localization to CEBPB target enhancer sites, Related to Figure 1. A. Known chromosomal breakpoints that produce FUS::DDIT3 oncoproteins in MLPS. **B.** Venn diagram of SMARCC1 and DDIT3 (FUS::DDIT3) MACS-called peaks in MLPS-1765-92 in the shSCR condition. **C.** Heatmap of DDIT3 (FUS::DDIT3), SMARCC1, H3K27ac, and ATAC-seq peaks over FUS::DDIT3 peaks in MLPS-1765-92 in the shSCR condition. **D**. Distance-to-TSS plots for FUS::DDIT3, SMARCC1, and sites with both FUS::DDIT3 and SMARCC1 in MLPS-1765-92 in the shSCR condition. **E.** mRNA levels (raw RPKMs) of Exons 1-4 of the *DDIT3* gene; Exon 1 is specific to wild-type *DDIT3*. **F.** Distance-to-TSS plots for SMARCC1 peaks gained and lost upon fusion knockdown in MLPS-1765-92. **G.** Heat map depicting DDIT3, SMARCC1, H3K27Ac, and ATAC-seq over n=1980 total BAF-gained sites following shDDIT3 treatment (fusion knockdown). **H.** Metaplot of DDIT3, SMARCC1, H3K27Ac, and ATAC-seq in shSCR (control, dotted line) and shDDIT3 (fusion knockdown, solid line) conditions. **I.** Schematic of important stages of adipogenesis with transcription factors that regulate adipogenesis indicated. **J.** ATAC-seq peaks in MLPS-1765-92 with shSCR and shDDIT3. **K.** ChromVar analysis of ATAC-seq peaks in MLPS-1765-92 treated with shSCR or shDDIT3 (2 replicates). **L.** Validation of FUS::DDIT3 knockdown at the protein level in MLPS-402-91 cells on day 14 post-transduction. **M.** Differential occupancy of BAF complexes (via SMARCC1 edgeR) on the genome upon FUS::DDIT3 knockdown in MLPS-402-91. **N.** LOLA of sites that gain BAF complexes upon FUS::DDIT3 knockdown in MLPS-402-91.

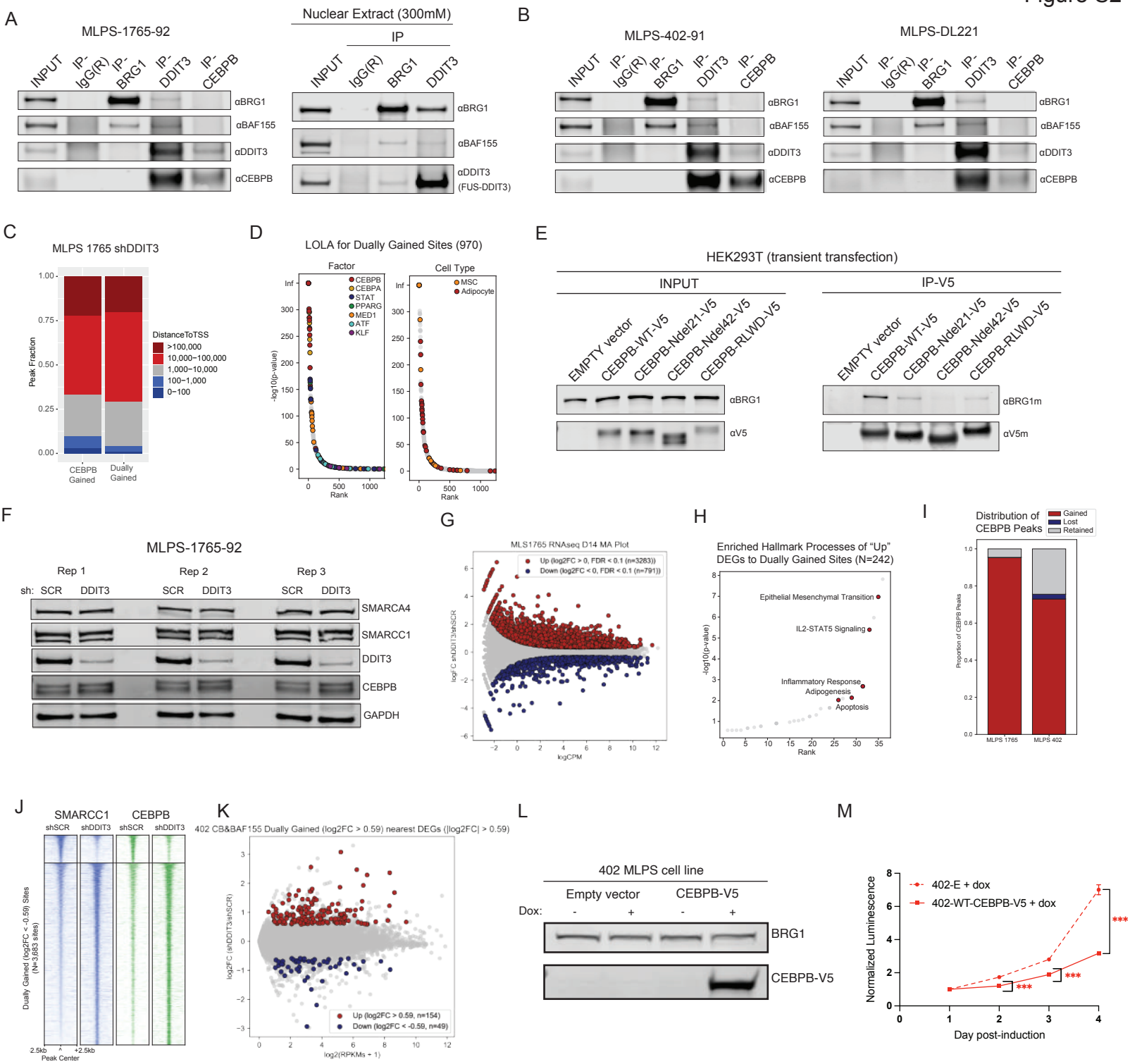

Figure S2. FUS::DDIT3 binds CEBPB, inhibiting its biochemical engagement and chromatin targeting of BAF complexes, related to Figure 2. A. (left) IP-WB for endogenous BRG1, DDIT3, and CEBPB in MLPS-1765-92; (right) IP-WB for endogenous BRG1 and DDIT3 in MLPS-1765-92. **B.** IP-WB for endogenous BRG1, DDIT3, and CEBPB in MLPS-402-91 and MLPS-DL221. **C.** Distance to TSS plots for sites that gain CEBPB and sites that dually gain CEBPB and SMARCC1 upon FUS::DDIT3 knockdown. **D.** LOLA of sites that dually gain SMARCC1 and CEBPB. **E.** Nuclear protein input and IP-WB for V5-tagged CEBPB wild-type and mutant variants. Ndel21, Ndel42 are CEBPB constructs lacking the first 21 or 42 aa, respectively. CEBPB-RLWD, RLWD-->AAAA (positions R3A, L4A, W7A, D8A) **F.** (left) Immunoblots reflecting total nuclear BAF complex subunit, DDIT3, CEBPB and GAPDH control levels in MLS-1765-92 cells treated with either shSCR or shDDIT3. (right) Bar graph indicating GAPDH-normalized densitometry of CEBPB immunoblots (n=3 experimental replicates). **G.** MA plot of RNA-seq data from MLPS-1765-92 cells upon FUS::DDIT3 knockdown. **H.** Gene ontology analysis of upregulated genes that are near dually gained sites across the Hallmark genesets. **I.** Proportion of gained, lost, and retained CEBPB peaks in MLPS-1765-92 and MLPS-402-91 upon FUS::DDIT3 knockdown. **J.** In MLPS-402-91, CEBPB is gained at sites that gain SMARCC1 upon FUS::DDIT3 knockdown (day 14 post-transduction). **K.** In MLPS-402-91, SMARCC1 and CEBPB are gained at sites on day 14 post-knockdown transduction that are near genes that are upregulated on day 7 post-knockdown transduction. **L.** Immunoblot performed on MLS 402 cells containing a dox-inducible system to overexpress C-terminally V5-tagged CEBPB. **M.** Proliferation curves demonstrating CEBPB-mediated attenuation of MLPS cell (402 cell line) proliferation (Cell-titer Glo, norm. luminescence).

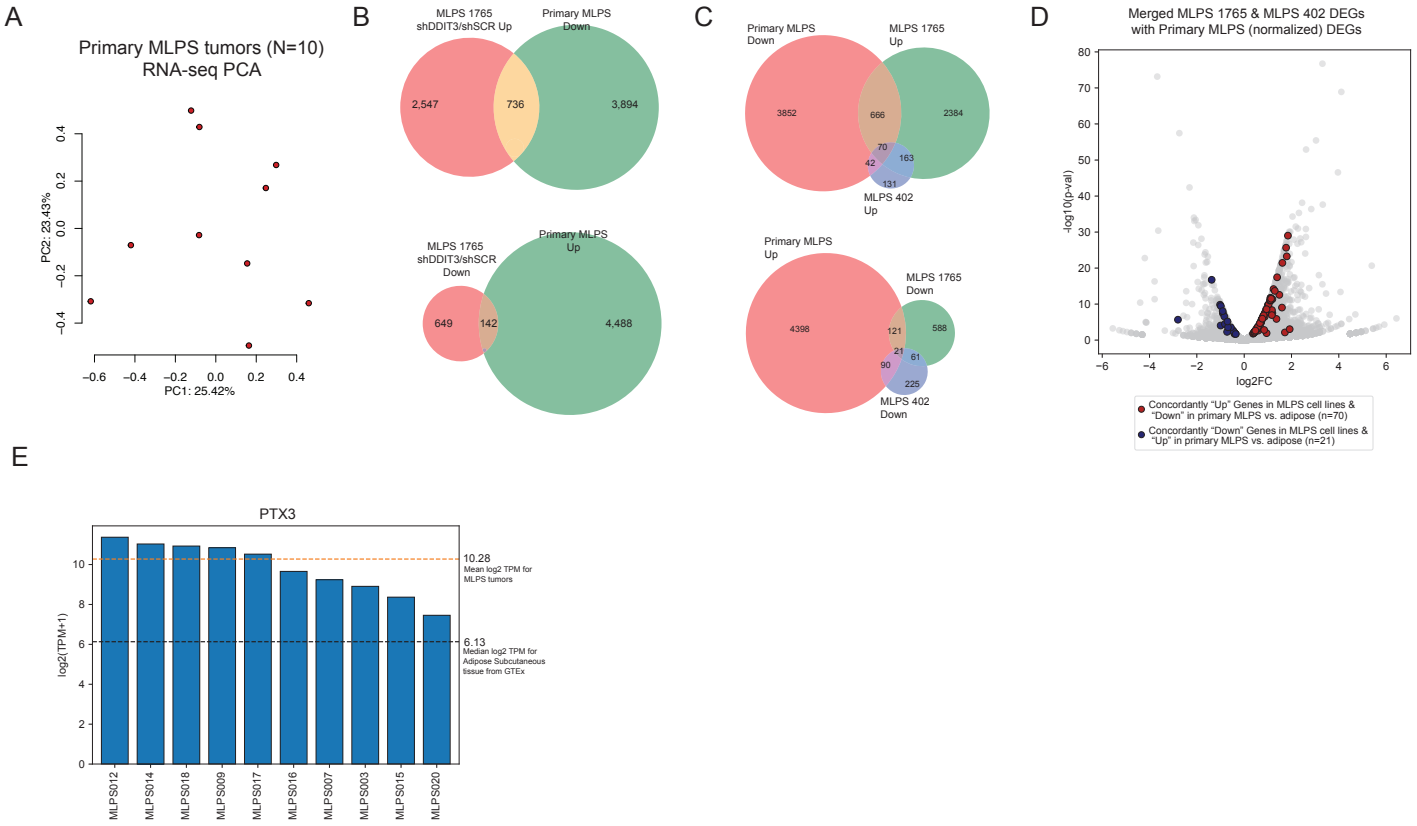

Figure S3. Gene regulatory analyses integrating primary MLPS tumor and MLPS cell line RNA-seq and chromatin binding studies, Related to Figure 3. A. PCA of gene expression from primary MLPS tumors. **B. (Top)** Venn diagram of genes upregulated upon FUS::DDIT3 knockdown in MLPS 1765 (MLPS 1765 shDDIT3/shSCR Up) and lowly expressed in primary MLPS tumors compared to primary adipose tissue; **(Bottom)** Venn diagram of genes downregulated upon FUS::DDIT3 knockdown in MLPS-1765 (MLPS1765 shDDIT3/shSCR Down) and highly expressed in primary MLPS compared to primary adipose tissue. **C. (Top)** Venn diagram of genes upregulated upon FUS::DDIT3 knockdown in MLPS-1765-92 & MLPS-402-91 and lowly expressed in primary MLPS tumors compared to primary adipose tissue; **(Bottom)** Venn diagram of genes downregulated upon FUS::DDIT3 knockdown in MLPS-1765-92 & MLPS-402-91 and highly expressed in primary MLPS compared to primary adipose tissue **D.** Genes differentially expressed in MLPS-1765-92 (shDDIT3/shSCR), MLPS-402-91 (shDDIT3/shSCR), and primary MLPS tumors (MLPS/adipose tissue). **E.** PTX3 expression in primary MLPS tumors compared to normal adipose tissue.

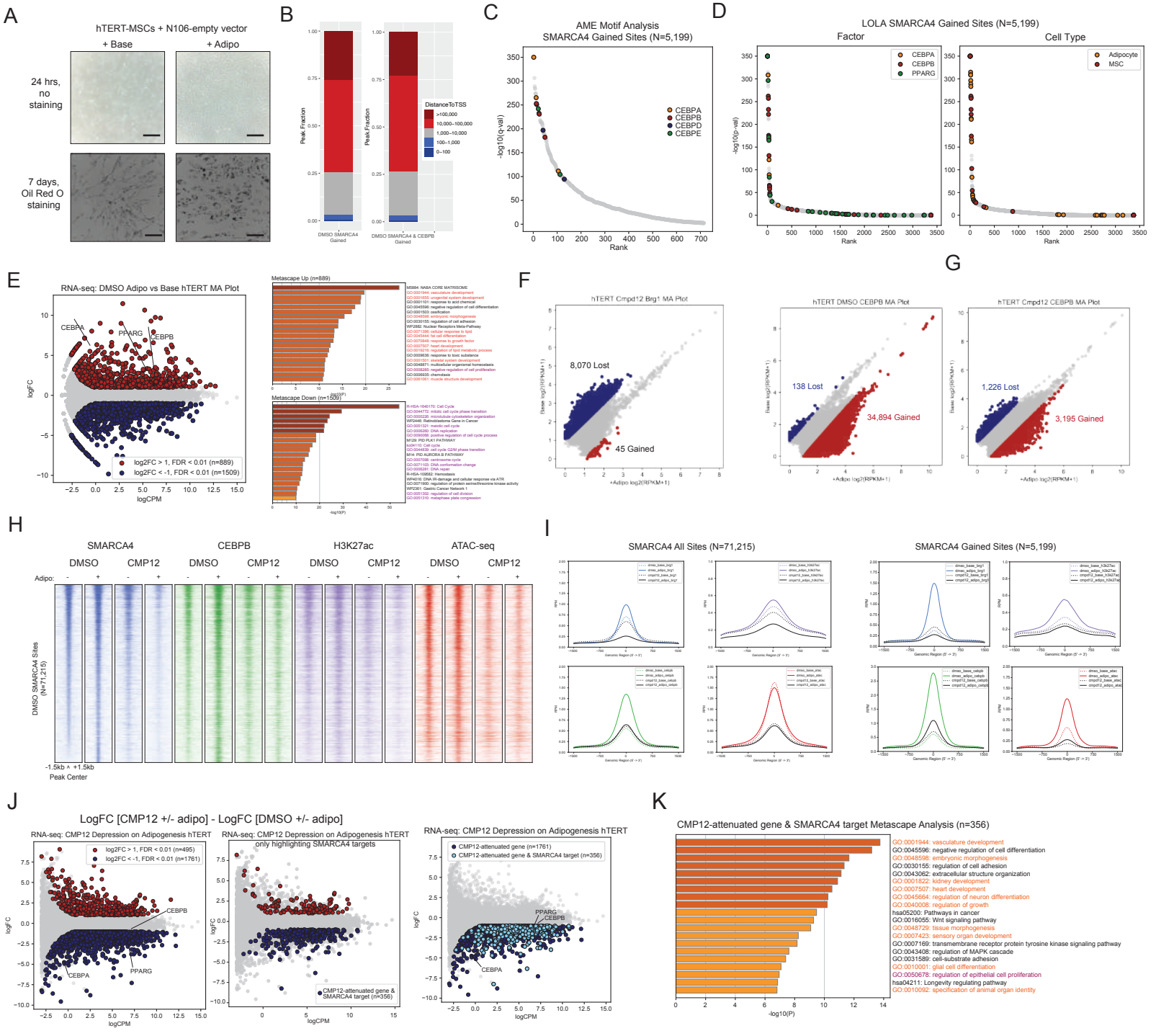

Figure S4. Small molecule inhibition of SMARCA4/SMARCA2 ATPase activity reveals BAF complex requirement during normal adipogenesis, Related to Figure 4. A. Morphology change and increased lipid droplets using StemPro Adipogenesis Differentiation kit in hTERT-MSCs (scale bar, 100 microns). **B.** Distance to TSS plot of sites that gain SMARCA4 only or SMARCA4 and CEBPB upon 24 hrs adipogenesis. **C.** AME motif analysis of SMARCA4 gained sites upon 24 hrs adipogenesis. **D.** LOLA of SMARCA4 gained sites upon 24 hrs adipogenesis. **E.** Changes in RNA expression upon adipogenesis with Metascape analysis. **F.** edgeR analysis of differential occupancy of BAF complexes (SMARCA4) on the genome upon 24 hours adipogenesis with CMP12 treatment. **G.** edgeR analysis of differential occupancy of CEBPB on the genome upon 24 hours adipogenesis with DMSO or CMP12 treatment. **H.** Heatmap & metaplots over all SMARCA4 peaks. **I.** Metaplots over all SMARCA4 peaks (left) and gained SMARCA4 peaks (right). **J.** LogFC [CMP12 +/- adipo] - LogFC [DMSO +/- adipo] showing attenuation of gene expression with CMP12 treatment. **K.** Metascape analysis of CMP12-attenuated genes and SMARCA4 targets.

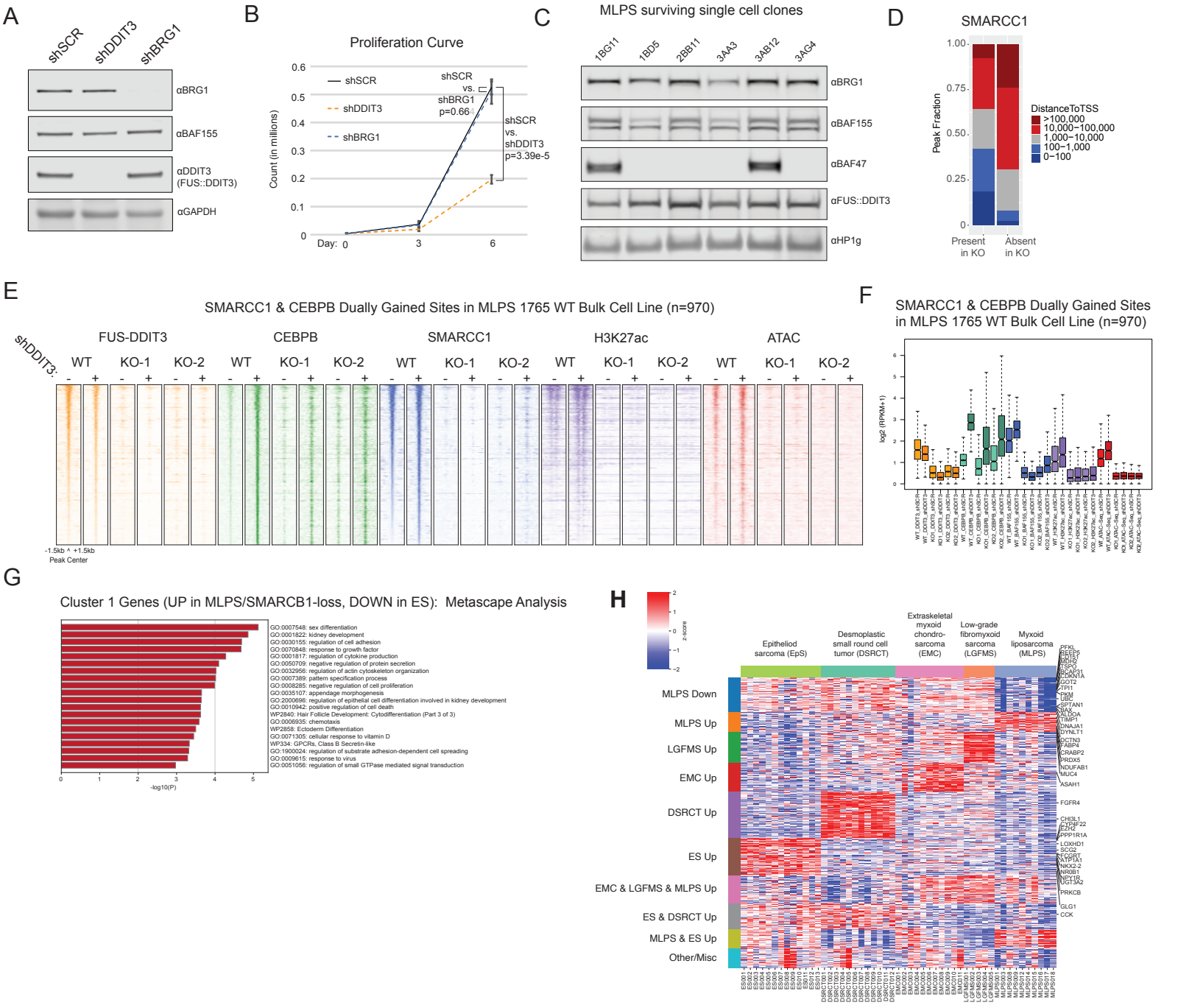

Figure S5. SMARCB1 loss prevents BAF complex and CEBPB retargeting upon FUS::DDIT3 suppression, Related to Figure 5. A. FUS::DDIT3 knockdown (shDDIT3) and BAF complex ATPase knockdown (shBRG1) in MLPS-1765-92 cells. **B.** Proliferation curve in MLPS-1765-92 cells demonstrating that shDDIT3 slows proliferation rate (p=3.39e-5), while shBRG1 does not (p=0.664).**C.** Screening of single cell MLPS- 1765-92 clones. **D.** Distance to TSS plots for SMARCC1 peaks in WT condition from Figure 5F that are present and absent in *SMARCB1*-KO clones. **E.** Heatmap demonstrating DDIT3 (FUS::DDIT3), CEBPB, SMARCC1 (BAF complex), and H3K27ac occupancy in the WT MLPS-1765-92 line compared to the *SMARCB1*-KO clones 1BD5/KO-1 and 3AA3/KO-2 over sites that dually gain SMARCC1 and CEBPB in the bulk WT MLPS-1765 line. **F.** Boxplots corresponding to heatmaps. **G.** Metscape analysis of genes in cluster 1 from K-means clustering heatmap of primary MLPS, MRT, RMC, and EpS tumors against primary ES tumors. **H.** K-means clustering analyses performed using all FET fusion samples (including MLPS, DSRCT, LGFMS), and EpS and using log2(TPMs+1) as input following selecting for top 10% most variable genes. Selected genes are indicated.